



HAL
open science

Synergistic or Antagonist Effects of Different UV Ranges Analyzed by the Combination Index: Application to DNA Photoproducts

Thierry Douki, Arnaud Buhot

► **To cite this version:**

Thierry Douki, Arnaud Buhot. Synergistic or Antagonist Effects of Different UV Ranges Analyzed by the Combination Index: Application to DNA Photoproducts. Photochemistry and Photobiology, In press, 10.1111/php.13528 . hal-03356359v1

HAL Id: hal-03356359

<https://hal.science/hal-03356359v1>

Submitted on 28 Sep 2021 (v1), last revised 11 Oct 2021 (v2)

HAL is a multi-disciplinary open access archive for the deposit and dissemination of scientific research documents, whether they are published or not. The documents may come from teaching and research institutions in France or abroad, or from public or private research centers.

L'archive ouverte pluridisciplinaire **HAL**, est destinée au dépôt et à la diffusion de documents scientifiques de niveau recherche, publiés ou non, émanant des établissements d'enseignement et de recherche français ou étrangers, des laboratoires publics ou privés.

Synergistic or Antagonist Effects of Different UV Ranges

Analyzed by the Combination Index: Application to DNA

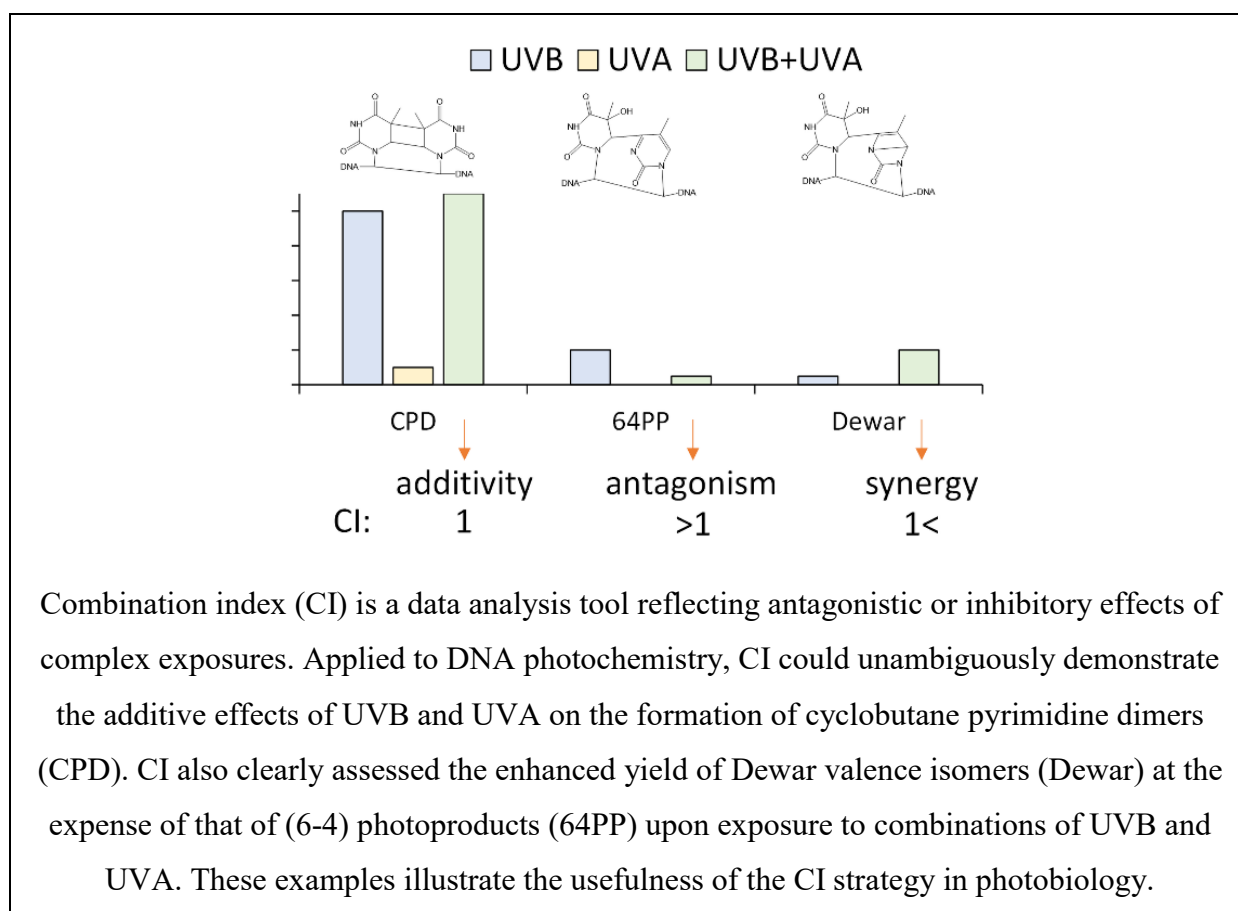
Photoproducts

Thierry Douki* and Arnaud Buhot

Univ. Grenoble Alpes, CEA, CNRS, IRIG, SyMMES, F-38000 Grenoble

Corresponding authors: Thierry Douki

Email: thierry.douki@cea.fr



18 **ABSTRACT**

19 Photobiological effects are known to greatly depend on the wavelength of the incident photons
20 that define the nature of the activated chromophores. A growing number of experimental data
21 show that considering the effect of complex light sources as a sum of the effects of
22 monochromatic exposures can be misleading. Indeed, the combined exposure to several
23 wavelength ranges may modulate photobiological responses or even induce novel processes.
24 These observations are similar to a well-known topic in chemical toxicology: the non-additivity
25 of effects in mixtures where either antagonism or synergy are often observed. In the present
26 work, we investigated if a data analysis tool first developed for studying non-additivity in
27 mixtures of drugs, the combination index, could be applied to photobiological processes. We
28 chose to work on the formation of UV-induced DNA photoproducts where additive, antagonist
29 and synergistic effects take place simultaneously. In addition to this application, we worked on
30 the mathematical bases of the concept in order to broaden its applicability to phenomena
31 exhibiting various dose-response patterns. We also addressed the question of the evaluation of
32 the error on the determination of the combination index.

33

34

35 Keywords: data modeling, co-exposure, action spectra, non-additive effects, DNA damage

36

37 INTRODUCTION

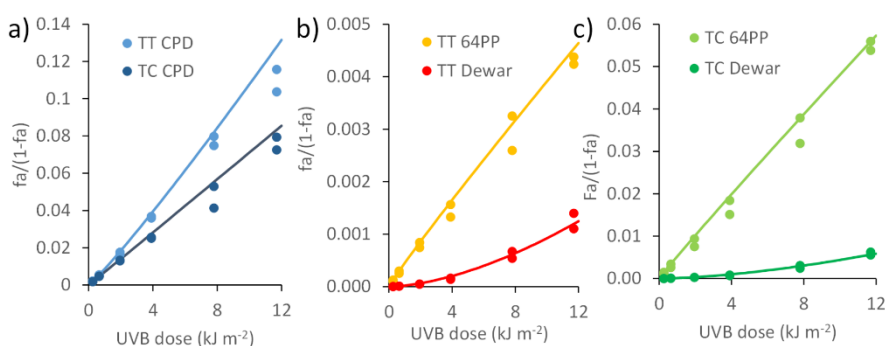
38 The activation and the intensity of photobiological responses are obviously dependent on the
39 fluence of the radiation but also of the wavelength of the incident photons. This has been
40 realized for a long time and is classically taken into account by the use of action spectra (1-4),
41 which report the wavelength-dependent variation of the intensity of an effect per dose unit. By
42 convolution with the emission spectrum of a source of interest, action spectra provide an
43 estimation of the biological effect under specific experimental conditions. However, the use of
44 action spectra is based on an additivity principle that is not always relevant in photobiology.
45 Some photobiological effects may result from the consecutive impact of two different
46 wavelength ranges. In this case, a synergy is observed. Conversely, there are cases where the
47 response triggered by a wavelength range is decreased by another, leading to an antagonism.
48 Examples can be found in the photomorphogenesis of plants that is activated and inhibited at
49 two different wavelengths, (5) or in bacteria where sunlight simultaneously induces DNA
50 damage and activates photolyase repair enzymes (6, 7). As we recently reviewed, similar
51 non-additive effects have been reported in humans and in mammalian cells (8).
52 Immunosuppression is induced by both UVB and UVA but UVA may counteract the effect of
53 UVB (9-11). Similarly, the extent of apoptosis depends on the ratio between the two wavelength
54 ranges upon co-exposure to UVB and UVA (12). More recently, UVA was reported to modulate
55 the cytotoxicity of UVB (13). Other examples concern the induction of oxidative stress. UVA
56 was found to promote the formation of lipofuscin that is a visible light photosensitizer (14).
57 Similarly, some UVB photoproducts of tryptophan like N-formylkynurenine are
58 UVA-photosensitizers (15-17). Last, in the field of DNA damage, pyrimidine (6-4) pyrimidone
59 photoproducts (64PPs) are produced by UVB radiation in DNA and efficiently converted into
60 their Dewar valence isomers (Dewars) by UVA photons (18, 19).

61 The non-additive effects of different wavelength ranges represent thus a key issue in the
62 prediction and understanding of photobiological effects. Unfortunately, they are not frequently
63 taken into consideration or only on a very limited number of applied doses. This last point is
64 important because some effects can be additive within a dose range and antagonist or synergistic
65 in another. The purpose of the present work is thus to provide a methodology for the
66 identification of non-additivity effects in photobiology under the largest set of conditions
67 possible with the most reasonable amount of experimental work. Ideas of experimental design
68 and data treatment for this problem can be found in the field of the pharmaceutical and
69 toxicological effects of chemicals, where examples of non-additive responses to the
70 combination of organic or inorganic compounds are countless. The question of the non-additive
71 effects has been put forward for many years with the notions of exposome and cocktail effects
72 (20). Several mathematical models have been designed to analyze experimental data and
73 establish the occurrence, or not, of synergy or antagonism in the impact of mixtures (21-23).
74 Among them, the combination index (CI) approach proposed by Chou (24-27) is particularly
75 attractive as it combines the *a priori* definition of an optimal experimental plan with a strict
76 mathematical approach for the identification of antagonist or synergistic effect. This strategy
77 was designed for the optimization of the efficiency of combinations of drugs. It was very
78 successful in various fields. More than 1500 references to the combination index could be
79 retrieved, for a large part in the field of cancer treatment but also in studies on HIV or in
80 toxicology investigations. The most complete review on the combination index (25) has
81 received more than 4000 citations. The mathematical model designed by Chou is derived from
82 the mass action law and is well suited to study the interaction of a drug with a physiological
83 target (25, 27). Extensive mathematical analysis of the underlying phenomena led Chou and his
84 co-workers to propose a rather simple equation describing pharmaco-kinetics interaction, the

85 medium effect equation (MEE). The same mathematical framework led to the design of the CI,
86 a convenient tool to study antagonist and synergistic effects.

87 As it originates from the mass action law, the MEE can precisely model data ranging between
88 0 and 1 (or 0 and 100 %) with dose-dependent curves of the responses exhibiting sigmoidal or
89 hyperbolic shapes. In addition, the MEE requires only two fitting parameters thus limiting the
90 required dose-response experiments for their determination. Determining the MEE is a requisite
91 to the calculation of the CI. The value of the CI shows whether the effects of a mixture are
92 additive ($CI=1$), antagonist ($CI>1$) or synergistic ($CI<1$). The strategy underlying the CI
93 approach is illustrated on a theoretical example on Scheme 1. In the framework designed by
94 Chou and co-workers, results are expressed as the affected fraction fa , namely the yield of a
95 process. Experiments are first performed with the two studied chemical or physical factors alone
96 in a series of doses or concentrations. The parameters of the MEE are calculated for each set of
97 data by a Log-Log transformation. More mathematical details are provided in the “Data
98 Modeling” part below. The CI can then be calculated for any combination of the two factors.
99 Obviously, it is of utmost importance to determine the CI over a wide variety of mixture
100 compositions, which drive the extent of deviation from additivity. Therefore, CI investigations
101 include a third experiment in which the two factors are applied simultaneously in different
102 concentrations but with a constant ratio. The global effect fx of each of these combinations
103 $D1+D2$ is determined. The MEE for the two factors are then used to determine the
104 concentration of the dose $Dx1$ and $Dx2$ of pure factors 1 and 2 necessary to induce the same
105 effect fx as the mixture. The CI is defined as $\frac{D1}{Dx1} + \frac{D2}{Dx2}$. Additivity is shown by a value of CI of
106 1. This can be illustrated by an example with two factors equally efficient at inducing a response
107 (same MEE). If a 1:1 mixture of factors 1 and 2 at a dose D induces a response fx , $Dx1$ value
108 will be $2D$ (because factor 1 alone is as efficient as factor 2 in the mixture). The same will be
109 obtained for factor 2. Therefore, $CI = \frac{D}{2D} + \frac{D}{2D} = \frac{1}{2} + \frac{1}{2} = 1$. Similar calculations can be made

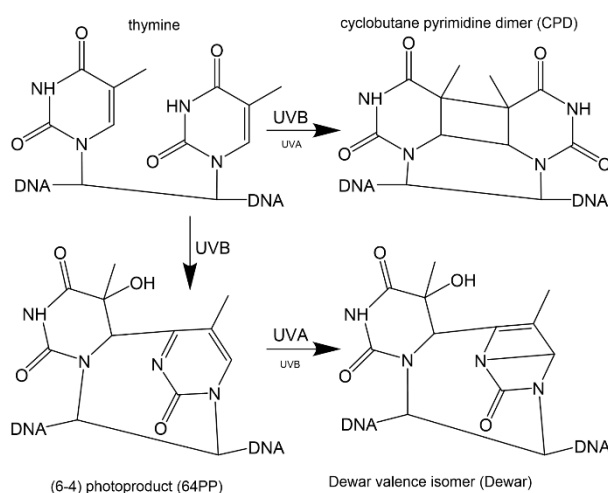
110 when factors 1 and 2 are not equally efficient. Keeping this example of equally efficient factors
 111 1 and 2, it may be observed in other cases that the dose of pure factor 1 or pure factor 2 required
 112 to observe a response f_x is less than $2D$. In this case the $\frac{D}{D_x}$ terms in CI are larger than $\frac{1}{2}$ and
 113 consequently $CI > 1$. This correspond to a situation where a larger amount of the two factors are
 114 necessary in mixture than as pure products to observe a same effect. This is typically the case
 115 of an antagonist mixture effect. An opposite calculation can be made for synergy effects that
 116 correspond to $CI < 1$.



117
 118 **Scheme 1:** Principle of the determination of the combination index CI . (a) The amplitude of
 119 the studied effect f_a is determined for factors 1 and 2 applied alone on a range of
 120 concentrations that can be different for the two factors. (b) Experiments are performed with
 121 mixtures of factors 1 and 2 exhibiting a constant ratio D_1/D_2 . The CI can be determined for
 122 each of the mixtures. Those have a concentration D_1+D_2 and induce an effect f_x . (c) Data from
 123 (a) are fitted by the MEE. The latter equation provides the values of the concentration of pure
 124 factors 1 (D_{x1}) and 2 (D_{x2}) leading to the effect f_x . (d) The CI is calculated and the
 125 conclusion on additivity, synergy or antagonism is deduced.

126
 127 In the present work, we aimed at providing a proof-of-concept that the CI approach could be
 128 used in photobiology. For this purpose, we applied the CI formalism to the well-known UV
 129 photochemistry of DNA (Scheme 2), and in particular to the formation of pyrimidine dimers
 130 (28-30). These photoproducts arise, upon exposure to UVB, from the cycloaddition of the
 131 C5-C6 double bonds of adjacent pyrimidine bases or from the addition of the C5-C6 double
 132 bond of the 3'-end pyrimidine to the C4 carbonyl or imine group of the 5'-end pyrimidine. The

133 respective products are cyclobutane pyrimidine dimers (CPDs) and 64PPs. CPDs are also
 134 produced by UVA, although in much lower amounts than by UVB. A specific feature of 64PPs
 135 is that their pyrimidone moiety can absorb a second UV photon and undergo photoisomerization
 136 into Dewars. In isolated photoproducts, this photoreaction is most efficient at approximately
 137 320 nm (31, 19, 32, 33), but this maximum is shifted towards the UVA region (18) within DNA
 138 because of the presence of overwhelming amounts of normal bases that shield UVB photons
 139 (34). DNA photochemistry thus offers examples of additive (CPDs), synergistic (Dewars) and
 140 antagonist (64PPs) effects between UVB and UVA. In addition, the yield of photoproducts
 141 cannot be more than 100 %. The latter observation is reinforced by the fact that experiments
 142 are always performed at a low modification rate that mimics real life situations. In that respect,
 143 these data are well suited for application of the MEE. We also used them to explore the use of
 144 other modeling equations in place of the MEE. Indeed, the latter function does not reproduce
 145 all possible dose-course shapes of biological responses, which can be more complex than a drug
 146 / target interaction. In addition, numerous effects do not range between 0 and 1, and can exhibit
 147 no theoretical limit.



148
 149 **Scheme 2:** Structure of the dimeric pyrimidine photoproducts induced in DNA by UVB and
 150 UVA. The photoreactions are described for two thymines but similar products can be formed
 151 at TC, CT and CC sequences.

152 **EXPERIMENTAL PART**

153 Irradiations were performed with high-grade calf thymus DNA (Sigma, Saint Quentin Fallavier,
154 France). A stock solution at approximately 1 mg mL^{-1} was prepared in deionized water (Milli
155 Q) and desalted by dialysis for 24 h in water with repeated changing of the water bath. The
156 solution was then diluted in an aqueous 50 mM NaCl solution at a DNA concentration of 50
157 $\mu\text{g mL}^{-1}$. It was then exposed to UV radiation in $1 \times 1 \times 4$ cm fluorimeter quartz cell (Hellma
158 Analytics, Munich, Germany). The irradiation set-up consisted of three lamps. A 2×15 W and a
159 15 W UVA lamps were placed facing perpendicular sides of the sample. Both lamps carried
160 T15-L Vilber-Lourmat tubes (Marne-La Vallée, France) exhibiting an emission spectrum
161 ranging from 320 to 380 nm with a maximum at 365 nm. A UVB lamp fitted with a 15W T15-M
162 tube exhibiting an emission centered at 312 nm (Vilber-Lourmat, Marne-La Vallée, France)
163 was placed on the opposite side of the 2×15 W UVA lamp. The UVA fluences were determined
164 with a Model 5.7 Solar meter (Solar Light, Glenside, PA). The UVB dosimetry was carried out
165 with a VLX 3W radiometer (Vilber Lourmat, Marne-la-Vallée, France) fitted with a 312 nm
166 probe. The sample holder could accommodate filters and was placed on a magnetic stirrer for
167 a constant homogenization of the sample during irradiation. For irradiation, the quartz cell was
168 loaded with 2.5 mL of DNA solution and, except for experiment 3 (see below), 200 μL aliquot
169 fractions were collected after increasing exposure times.

170 Four series of experiments were performed with different designs. Only the UVB and the 2×15
171 W UVA lamps used in the three first series while the 3 lamps were used in the last.

172 1) A filter with cut-off at 320 nm (Schott, Colombes, France) was placed in front of the
173 samples in the UVA beam. The fluences were constant and set at $0.13 \text{ kJ m}^{-2} \text{ min}^{-1}$ for
174 UVB and $2.36 \text{ kJ m}^{-2} \text{ min}^{-1}$ for UVA. Exposure times ranged between 1 and 90 min,
175 and the experiments were repeated twice.

- 176 2) The fluence of the UVA source (with a cut-off filter at 320 nm) was left constant at 0.65
177 $\text{kJ m}^{-2} \text{min}^{-1}$. The position of the UVB lamp (with a cut-off filter at 295 nm, Schott,
178 Colombes, France) was changed to provide fluences of either 0.20, 0.16, 0.12, 0.09 or
179 $0.03 \text{ kJ m}^{-2} \text{min}^{-1}$. Irradiations were performed once under each UVB conditions with
180 exposure times ranging between 4 and 64 min. Samples were analyzed once except that
181 receiving the largest dose which was analyzed three times. The values for this sample
182 were averaged before data analysis.
- 183 3) UVB and UVA fluences (with cut-off filters at 295 and 320 nm, respectively) were kept
184 constant at 0.08 and $0.73 \text{ kJ m}^{-2} \text{min}^{-1}$, respectively. Five irradiation protocols were
185 used. DNA samples (2 mL) were irradiated for either 5, 10, 20 or 40 min. Three aliquot
186 fractions (200 μL) were collected from each of these UV-exposed solutions. The three
187 first protocols involved either UVA, UVB or UVB and UVA simultaneously. In the
188 fourth design, samples were exposed for 5 min to pure UVA and then for 5 min to UVB.
189 The experiment was repeated with consecutive exposures to UVA and UVB lasting
190 10+10, 20+20 or 40+40 min. The fifth protocol was similar except that UVB was
191 applied before UVA. All these experiments were referred to as UVA, UVB,
192 UVB+UVA, UVA \rightarrow UVB and UVB \rightarrow UVA. Each irradiation was performed once but
193 all collected samples were analyzed three times and the obtained results were averaged
194 before data analysis.
- 195 4) The three lamps were used with bandpass filters of 310 ± 5 nm for UVB, 340 ± 13 nm for
196 the 1×15 W UVA and 386 ± 13.5 nm for 2×15 W UVA. All bandpass filters were
197 obtained from Edmund Optics (Lyon, France). The respective fluences were 0.0048,
198 0.036 and $0.045 \text{ kJ m}^{-2} \text{min}^{-1}$, respectively. Irradiation lasted 30, 60, 90 and 120 min.
199 The experiment was repeated three times.

200 Following irradiation, DNA was precipitated from the samples by addition of NaCl and
201 cold ethanol. The level of photoproducts was then determined as previously reported (35).
202 The DNA samples were enzymatically hydrolyzed by phosphodiesterases, DNases and
203 alkaline phosphate. The resulting solutions were analyzed by high performance liquid
204 chromatography coupled to tandem mass spectrometry.

205 **DATA MODELING**

206 All calculations were performed in Microsoft Excel spread sheets in order to copy and paste
207 data directly from the software of the LC-MS/MS system. We determined the values of the
208 parameters of the MEE (D_m and m), of the D_x and of CI using the method described by Chou
209 (25, 27). We used Compusyn (ComboSyn Incorporated) on a subset of data to check that our
210 calculations were correct. Excel sheets were also used for the calculation of the CI using other
211 equations with the first set of experimental results. Values of the coefficients of the regressions
212 and of their error were obtained from Origin (OriginLab Corporation, MA). For the calculation
213 of the propagation of errors, we used the classical method stating that if a measure y is a function
214 of a parameter x , then $\Delta y = \left| \left(\frac{df}{dx} \right) \right| \times \Delta x$, where Δy and Δx are the errors on y and x , respectively.

215 When y depends on more than one parameter, the absolute values of all errors are added: $\Delta y =$
216 $\left| \left(\frac{df}{dx_1} \right) \right| \times \Delta x_1 + \left| \left(\frac{df}{dx_2} \right) \right| \times \Delta x_2 + \left| \left(\frac{df}{dx_3} \right) \right| \times \Delta x_3 + \dots$

217 **Medium effect equation**

218 The MEE used in the original work by Chou et al. (25) is the following:

$$219 \quad (1) \frac{fa}{(1-fa)} = \left(\frac{D}{Dm} \right)^m$$

220 where fa is the response referred to as affected fraction in the framework of drug/target
221 interactions, D the dose, Dm the dose leading to a 50% of the maximal effect, and m a coefficient

222 reflecting the shape of the curve ($m > 1 \rightarrow$ hyperbolic; $m = 1 \rightarrow$ sigmoidal; $m < 1 \rightarrow$ “flat”
 223 sigmoidal).

224 The Dm and m parameters were determined from the experimental data by linear regression of
 225 Log-Log curve

$$226 \quad (2) \quad \text{Log}\left(\frac{fa}{1-fa}\right) = f(\text{Log}(D)) = a \times \text{Log}(D) + b = m \times \text{Log}(D) - m \times \text{Log}(Dm)$$

227 m is thus the slope a and Dm is $10^{-\frac{a}{b}}$.

228 Calculation of the CI requires the determination of the dose Dx of each factor leading to the
 229 same effect fx than a given mixture. In other words, it is necessary to invert the MEE equation

230 (1) to determine Dx for a measured effect fx , a known value of $\frac{fa}{1-fa}$:

$$231 \quad (3) \quad Dx = Dm \times [fx]^{1/m}$$

232

233 The error on Dx (ΔDx) can be inferred from that on m and Dm . The coefficients m and Dm were
 234 obtained by linear regression of equation (2). Thus, $\Delta m = \Delta a$ is the estimated error on the slope
 235 a and ΔDm can be shown to be:

$$236 \quad (4) \quad \Delta Dm = \left(\left|\frac{1}{m}\right| \times \Delta b + \left|\frac{b}{m^2}\right| \times \Delta m\right)$$

237 The errors ΔDm and Δm can then be used to calculate the error on the determination of the dose
 238 Dx . When replicates of a same experiment are used, the mean \overline{fx} is associated to the standard
 239 deviation σfx used as an estimation of Δfx :

$$240 \quad (5) \quad \Delta Dx = \left|\overline{fx}^{-\frac{1}{m}}\right| \times \Delta Dm + \left|\frac{Dm \times \ln(\overline{fx})}{m^2} \times \overline{fx}^{-\frac{1}{m}}\right| \times \Delta m + \left|\frac{Dm}{m} \times \overline{fx}^{-\left(\frac{1}{m}-1\right)}\right| \times \Delta fx$$

241 In the present work, fa is the level of DNA photoproducts. In contrast to most works in the field
 242 of chromatographic detection of DNA damage, results were not expressed in number of damage
 243 per million normal bases but in ratio of mol of damage per mol of DNA bases. The values are

244 thus very small but range between 0 and 1 as necessary for the use of the MEE. In addition, the
 245 fa values used in the calculations with the MEE were normalized to the content of bipyrimidine
 246 sites at the origin of each photoproducts. For this purpose, we took into account the frequency
 247 of the different bipyrimidine dinucleotides in CT-DNA, which are 0.099, 0.061, 0.053 and
 248 0.053 for TT, TC, CT or CC, respectively (36, 37).

249 **Polynomial fit**

250 Calculation of the CI was also performed with polynomial fits of the DNA damage data. For
 251 this part of the work, results were expressed in number of photoproduct per million normal
 252 bases.

253 For Dewars, the experimental data were fitted using a second order polynomial equation.
 254 Because no photoproduct is detected in non-exposed DNA, the origin was set to 0. The
 255 expression is thus the following:

$$256 \quad (6) \quad fa = a \times D^2 + b \times D$$

257 The dose Dx necessary for the induction of an effect fx is the positive solution of equation (6):

$$258 \quad (7) \quad Dx = \frac{-b + \sqrt{b^2 + 4 \times a \times fx}}{2 \times a}$$

259 with the error of Dx being:

$$260 \quad (8) \quad \Delta Dx = \left| \frac{\overline{fx}}{a \sqrt{b^2 + 4 \times a \times \overline{fx}}} - \frac{\sqrt{b^2 + 4 \times a \times \overline{fx}}}{2a^2} \right| \times \Delta a + \left| \frac{1}{2a} \times \left(\frac{b}{\sqrt{b^2 + 4 \times a \times \overline{fx}}} - 1 \right) \right| \times \Delta b + \left| \frac{1}{\sqrt{b^2 + 4 \times a \times \overline{fx}}} \right| \times \Delta fx$$

261

262 Data for CPDs and 64PPs were fitted by a linear regression $f = a \times D$. In this case

$$263 \quad (9) \quad Dx = \frac{\overline{fx}}{a}$$

264 and the error is

265 (10) $\Delta Dx = \left| \frac{\overline{fx}}{a^2} \right| \times \Delta a + \left| \frac{1}{a} \right| \Delta fx$

266 **Kinetic analysis**

267 Another strategy for the determination of Dx involved a precise kinetic analysis. Because the
 268 level of damage was low, we considered that the DNA amount remained constant (DNA_0) and
 269 set to $DNA_0=10^6$ bases.

270 **CPD**

271 The formation of CPD in DNA was described as a single first order kinetic reaction.

272 (11) $CPD = DNA_0 \times (1 - e^{-k \times D})$

273 For the determination of a dose Dx leading to a specific level of CPD (fx):

274 (12) $Dx = -\frac{1}{k} \times \ln\left(1 - \frac{fx}{DNA_0}\right)$

275 The error on this value is thus:

276 (13) $\Delta Dx = \left| \frac{1}{k \times (1 - \overline{fx})} \right| \times \Delta fx + \left| \frac{\ln\left(1 - \frac{\overline{fx}}{DNA_0}\right)}{k^2} \right| \times \Delta k$ where \overline{fx} is the mean value of the level of CPD in a

277 co-exposure experiment and Δk the estimated error on the rate k .

278 **64PP and Dewar**

279 Formation of 64PP and Dewar results from two consecutive first order reactions
 280 $DNA \rightarrow 64PP \rightarrow Dewar$ with rate constants $k1$ and $k2$ respectively (38).

281 (14) $64PP = DNA_0 \times k1 \times \frac{e^{-k1 \times D} - e^{-k2 \times D}}{k2 - k1}$

282 (15) $Dewar = DNA_0 \times \frac{[1 - (k2 \times e^{-k1 \times D} - k1 \times e^{-k2 \times D})]}{k2 - k1}$

283 For the calculation of $k1$, we considered that all 64PPs produced at a given dose are either in
 284 their initial 64PP forms or as Dewars. Therefore, the sum of the levels of 64PP and Dewar can
 285 be described, like CPD, by a first order equation with a reaction constant $k1$.

286 (16) $(64PP + Dewar) = DNA_0 \times (1 - e^{-k_1 D})$

287 Log conversion and linear regression yielded the value of k_1 .

288 For k_2 , we converted the exponentials in equation (15) by a second order limited development:

289 (17) $Dewar = DNA_0 \times \frac{k_1 \times k_2 \times D^2}{2}$

290 Linear regression of the data with respect to D^2 provided a fair estimation of k_2 .

291 The dose Dx required for a specific level of Dewar ($f(x)$) can be determined from equation (18):

292 (18) $Dx = \sqrt{\frac{2 \times \overline{f(x)}}{DNA_0 \times k_1 \times k_2}}$

293 The error on this value is thus:

294 (19) $\Delta Dx = \frac{\left| \frac{1}{k_1 \times k_2} \right| \times \Delta f(x) + \left| \frac{-\overline{f(x)}}{k_2 \times k_1^2} \right| \times \Delta k_1 + \left| \frac{-\overline{f(x)}}{k_2^2 \times k_1} \right| \times \Delta k_2}{DNA_0 \times \sqrt{\frac{2 \times \overline{f(x)}}{k_1 \times k_2 \times DNA_0}}}$

295 For the determination of Dx for 64PPs, we first applied a second order limited development of
 296 the exponential functions in equation (14), and obtained equation (20):

297 (20) $64PP = DNA_0 \times k_1 \times D - DNA_0 \times \frac{k_1 \times (k_1 + k_2)}{2} \times D^2$

298 The dose Dx necessary for the induction of a defined level of 64PP ($f(x)$) is thus the solution
 299 (equation 21) of a second order equation that can be described as the ratio of 2 functions A and
 300 B :

301 (21) $Dx = \frac{(-k_1 \times DNA_0 + \sqrt{((k_1 \times DNA_0)^2 - 2 \times \overline{f(x)} \times (k_1^2 + k_1 \times k_2) \times DNA_0)})}{-(k_1^2 + k_1 \times k_2) \times DNA_0} = \frac{A}{B}$

302 The other solution of (20), $\frac{(-k_1 \times DNA_0 - \sqrt{((k_1 \times DNA_0)^2 - 2 \times \overline{f(x)} \times (k_1^2 + k_1 \times k_2) \times DNA_0)})}{-(k_1^2 + k_1 \times k_2) \times DNA_0}$, provided aberrant values
 303 (maximum Dx for $f(x)=0$ and then decreasing Dx for increasing $f(x)$).

304

305 Calculation of errors requires the derivation of Dx with respect to the $k1$, $k2$ and fx .

306 Consequently, we calculated dA and dB for each of these 3 parameters:

$$307 \quad (22') \quad dA(k1) = -DNA_0 + \frac{k \times DNO_0^2 + \overline{fx} \times DNA_0 \times (2k1 + k2)}{\sqrt{k1^2 \times DNA_0^2 - 2 \times \overline{fx} \times (k1^2 + k1 \times k2) \times DNA_0}}$$

$$308 \quad (22'') \quad dA(k2) = \frac{-\overline{fx} \times DNA_0 \times k1}{\sqrt{k1^2 \times DNA_0^2 - 2 \times \overline{fx} \times (k1^2 + k1 \times k2) \times DNA_0}}$$

$$309 \quad (22''') \quad dA(fx) = \frac{-(k1^2 + k1 \times k2) \times DNA_0}{\sqrt{k1^2 \times DNA_0^2 - 2 \times \overline{fx} \times (k1^2 + k1 \times k2) \times DNA_0}}$$

$$310 \quad (23') \quad dB(k1) = -(2k1 + k2) \times DNA_0$$

$$311 \quad (23'') \quad dB(k2) = -k1 \times DNA_0$$

312 Combination of equations (22') to (23'') provided the error on Dx :

$$313 \quad (24) \quad \Delta Dx = \left| Dx \times \left(\frac{dA(k1)}{A} - \frac{dB(k1)}{B} \right) \right| \times \Delta k1 + \left| Dx \times \left(\frac{dA(k2)}{A} - \frac{dB(k2)}{B} \right) \right| \times \Delta k2 + \left| Dx \times \frac{dA(fx)}{A} \right| \times \Delta fx$$

314 **Combination index**

315 The Combination Index CI was calculated for each experiment involving combination of UVB
316 and UVA using equation (25):

$$317 \quad (25) \quad CI = \frac{D_{UVB}}{D_{UVBx}} + \frac{D_{UVA}}{D_{UVAx}}$$

318 with D_{UVB} and D_{UVA} representing the doses of UVB and UVA radiation applied to the sample
319 in the combination experiments, and D_{UVBx} and D_{UVAx} the doses of pure UVB and UVA
320 inducing the same effect fx as the combination ($D_{UVB} + D_{UVA}$). D_{UVBx} and D_{UVAx} were calculated
321 using either equation (3), (7), (9), (12), (18) or (21) depending on the data modeling used and
322 the photoproduct considered.

323 Using the estimated errors ΔDx calculated for UVB and UVA alone (equations (5), (8), (10),
324 (13), (19) or (24)), and the dose D of UVB and UVA used in the combined exposure, the error
325 on CI was:

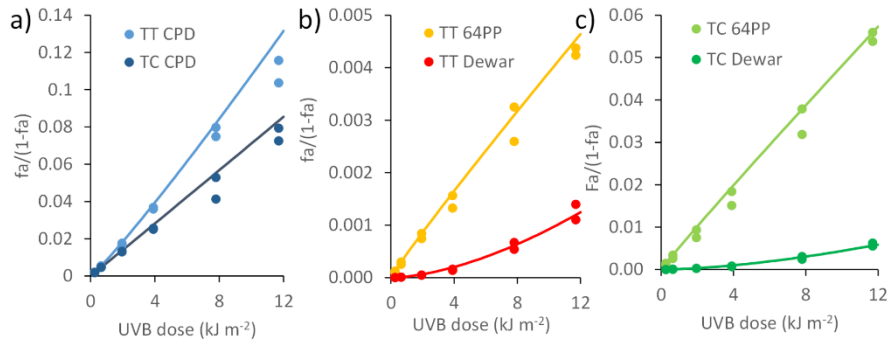
326
$$(26) \Delta CI = \left(D_{UVB} \times \frac{\Delta DUVBx}{DUVBx^2} \right) + \left(D_{UVA} \times \frac{\Delta DUVAx}{DUVAx^2} \right)$$

327 **RESULTS AND DISCUSSION**

328

329 **Effects of UVB and UVA co-exposure shown by the Combination Index and the**
330 **Median Effect Equation.**

331 In a first experiment, we investigated the effect of a combined exposure to UVB and UVA
332 through the classical *CI* approach with a modeling of the pure UVB and UVA data with the
333 MEE. DNA samples in aqueous solution were exposed to increasing doses of UVB (0.3-12 kJ
334 m⁻²) or UVA (5-212 kJ m⁻²). In a third experiment, DNA was exposed simultaneously to the
335 same increasing doses of UVB and UVA as those applied alone. The overall UV dose ranged
336 thus between 5.3 and 223 kJ m⁻². The parameters of the MEE, which are necessary to the
337 determination of the *Dx* values used in the calculation of the *CI* value, were calculated for UVB
338 for 8 photoproducts: TT CPD, TT 64PP, TT Dewar, TC CPD, TC 64PP, TC Dewar, CT CPD
339 and CC CPD. As previously reported, CC CPD, 64PPs and Dewars were not detected in the
340 samples exposed to UVA with our specific and sensitive HPLC-MS/MS assay (39-41).
341 Therefore, the MEE was determined for UVA only for TT CPD, TC CPD and CT CPD. The fit
342 of UVB data are shown on figure 1. The MEE slightly deviated from the experimental data for
343 CPDs at the largest UVB dose but nicely reproduced the shape of the dose curve formation of
344 64PPs and Dewars. A larger scattering was observed for UVA (data not shown) but the impact
345 of these values on the final *CI* is very low.

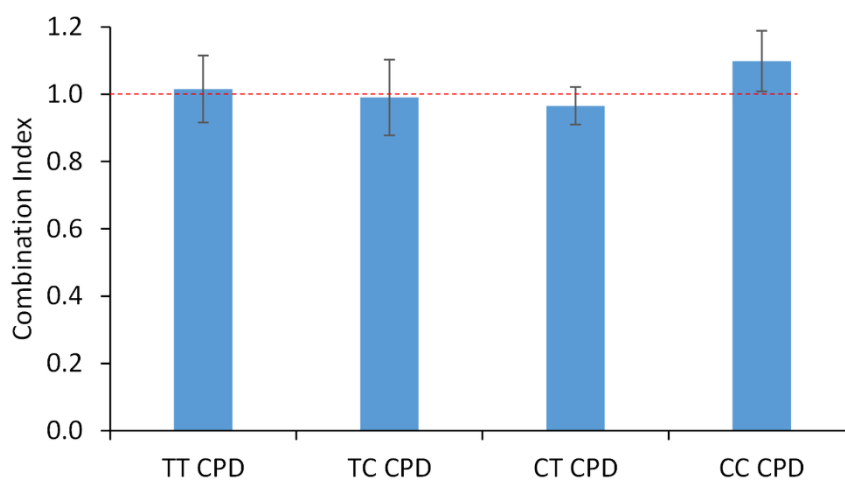


346

347 **Figure 1:** Fit of the dose-dependent formation of pyrimidine dimers in DNA exposed to UVB
 348 alone by the median effect equation (MEE) for a) TT and TC CPDs, b) TT 64PP and Dewar
 349 c) TC 64PP and Dewar. The marks represent the experimental data while the plain lines are
 350 the MEE fits.

351 These fits of the data were then used to calculate the *CI* for the different doses of combined
 352 UVB+UVA radiation. We were faced with lack of formation of 64PPs and Dewars in the
 353 samples exposed to UVA only. This situation is not *a priori* compatible with the calculation of
 354 *CI* where the ratio $\frac{D}{Dx}$ is taken into account for both factors. To overcome this limitation, we
 355 reasoned that a lack of formation could be seen as the necessity to apply an infinite dose to
 356 induce an effect. Consequently, the *Dx* value in the ratio involved in the calculation of *CI* is
 357 infinite and the ratio is null. We thus did not consider the term $\frac{D_{UVA}}{D_{UVAx}}$ in the calculation of *CI*
 358 for 64PPs, Dewars and CC CPD. Another improvement of the *CI* formalism in the present study
 359 was the accurate estimation of the error of the value of *CI*. A possible approach could be a
 360 replication of the whole experiment and the calculation of the mean and the variance. However,
 361 such an approach is not satisfactory because it does not really take into account the error on the
 362 MEE parameters and mostly reflects the variation in the results of the combination experiment.
 363 Therefore, we rather took into account the propagation of the estimated errors of the fitted
 364 parameters of the linear regression aimed at calculating the *m* and *Dm* coefficients of the MEE.
 365 A first observation regarding the calculated *CI* in this experiment was that the values were
 366 similar at all doses and close to 1 for the four studied CPDs (Fig. 2). This reflects that, in the

367 UVB and UVA ranges applied, formation of CPDs is a simple first order reaction. The
368 photoreversion observed with UVC radiation (42, 43), which is explained by a residual
369 absorption by CPD of these high-energy photons, does not take place. The present results also
370 confirmed that UVA induces the formation of T-containing CPDs but in much lower yield than
371 UVB. The observed ratio here was approximately 2000 for TT CPD. Consequently, additivity
372 is observed for CPD in case of co-exposure to UVB and UVA and the *CI* value is 1.



373
374 **Figure 2:** *CI calculated for CPD upon exposure of DNA to UVB and UVA in a 1:18 ratio.*
375 *The reported values are the means (\pm standard deviation) of results obtained in duplicate at*
376 *six different UV doses.*

377 In contrast to the formation of CPDs, the formation of 64PPs and Dewars was greatly affected
378 by the presence of UVA during UVB irradiation. 64PPs are efficiently produced by UVB but
379 not UVA. Both UVB and UVA are absorbed by the pyrimidone ring of 64PPs and convert them
380 into Dewars. In isolated 64PPs like photoproducts of dinucleoside monophosphates, this
381 reaction exhibits a maximal efficiency in the UVB range as 64PPs have a maximal absorption
382 at approximately 320 nm (31, 19, 32, 33). However, UVA is more efficient than UVB at
383 photoisomerizing 64PPs in DNA because of the shielding effects of the overwhelming amount
384 of the normal bases in the latter wavelengths range. This is observed in isolated as well as in
385 cellular DNA (34) and could be modeled based on available absorption features and quantum

386 yield data (18). The calculated *CI*s for the TT and TC 64PPs and Dewars unambiguously reflect
387 this chain of reactions (Table 1). The value of the *CI* is below 1 for Dewars. The mean value
388 was 0.3 and 0.4 for TT Dewar and TC Dewar, respectively, and thus corresponds to a synergy
389 effect in the combined exposure, namely a favored formation in the presence of UVA. The
390 opposite trend is observed for 64PPs since their *CI* are larger than 1. The *CI* analysis even
391 reflects known differences between the photochemistry of TC and TT 64PPs. The antagonism
392 of the formation of 64PP by UVA and the synergistic formation of Dewar are stronger for the
393 TT than the TC photoproducts. Actually, it was observed, from isolated DNA (44) to
394 mammalian cells (45, 46) and marine microorganisms collected on the field (47), that the yield
395 of conversion into Dewars was larger for TT 64PP than TC 64PP. The quantum yield for the
396 two photoisomerization reactions are similar with values of $2.0 \cdot 10^{-4}$ and $1.8 \cdot 10^{-4}$, respectively
397 (33). The absorption coefficient of TC 64PP is 3 times lower than that of TT 64PP (48), which
398 partly explains the difference in the yield of photoisomerization. A maximum absorption is
399 observed at 325 nm for TT 64PP (19) and 315 nm (32) for TC 64PP. Therefore, the lower
400 absorption coefficient of TC 64PP is compensated by the emission of the UVB source used in
401 this work that exhibits a maximum at 312 nm. More interesting for the topic of our work is that
402 calculations based on known absorption coefficients and quantum yields provided evidence that
403 the photoisomerization yield of TC 64PP is still 3-fold lower than that of TT 64PP in
404 combination of 300 and either 315, 320 or 340 nm light (34). This larger synergy in the
405 isomerization of TT 64PP compared to TC 66PP is reflected by the lower value of *CI* for TT
406 Dewar than TC Dewar. Another observation is the increase in the value of the *CI* of 64PPs
407 when the applied dose increased. This feature may be explained by the fact that, upon exposure
408 to combination of UVB and UVA, the level of 64PPs tends to a plateau while the increase is
409 more monotonous with pure UVB. Consequently, the antagonist effect is more pronounced
410 when the dose increases. Regarding the error on the determination of the *CI*, a general trend

411 observed for all photoproducts is that it is larger at the lowest doses. This can be explained by
 412 a less accurate determination of the amount of photoproducts or a less reproducible applied UV
 413 dose. In addition, the weight of the low values at the lowest dose is lower than that at high dose
 414 in the regression providing the parameters of the MEE. It is thus expected that the accuracy is
 415 lower at low dose.

416 **Table 1:** Values of the combination index (CI) determined for increasing doses of UVA and
 417 UVB applied in a 18:1 ratio. The reported total UV dose is expressed in kJ m^{-2} . The errors were
 418 obtained as described in the calculation section and included errors on the parameters of the
 419 MEE and the Dx dose.

CI calculated by the Median Effect Equation						
UV dose	TT 64PP	TT Dewar	TC 64PP	TC Dewar	TT CPD	TC CPD
5	1.12±0.63	0.32±0.11	1.23±0.75	0.44±0.20	0.83±0.12	0.83±0.23
12	1.27±0.57	0.31±0.12	1.28±0.67	0.48±0.22	0.99±0.18	0.87±0.23
37	1.53±0.71	0.29±0.08	1.33±0.62	0.45±0.19	1.13±0.21	1.05±0.29
75	2.04±0.96	0.28±0.08	1.30±0.73	0.38±0.16	1.07±0.15	1.03±0.26
149	3.30±1.65	0.30±0.08	1.44±0.74	0.34±0.13	1.03±0.16	1.09±0.44
223	4.75±2.34	0.33±0.08	1.69±0.82	0.32±0.10	1.04±0.19	1.07±0.30

420

421 The results clearly show that calculation of the CI based on the MEE as defined by Chou (25)
 422 is well suited for establishing additive or non-additive effects in photochemically-induced
 423 processes like formation of DNA damage. CI nicely reflects the additivity between UVB and
 424 UVA in the induction of CPDs, the lower levels of 64PPs in the presence of UVA and the larger
 425 amounts of Dewars upon co-exposure to UVB and UVA. The present work illustrates the ease
 426 of the procedure that requires only three experiments with a few doses to obtain an indication
 427 on the occurrence of synergistic or antagonist effects over a wide range of doses. In the present
 428 work, we could explore a dose range corresponding to a factor of 45 between the lowest and
 429 the largest dose with only 6 points for UVB, UVA and UVB+UVA.

430 **Calculation of *CI* with other fitting functions**

431 The results presented above for UVB and UVA is an illustration, in addition to countless
432 examples with drugs and chemical, of the power of the *CI* approach to identify synergism and
433 antagonism in mixtures. The definition of this parameter was inferred from extensive theoretical
434 work based on the mass action law and the concept of the MEE. Yet, the MEE was designed
435 for drug-target interactions and cannot reflect all possible biological responses. This is the case
436 for all the cellular processes that do not exhibit a dose-response shape with a plateau and that
437 cannot be normalized between 0 and 1. An important example is that of gene expression that
438 can be larger than one when increased with respect to a control sample and that do not have a
439 theoretical upper limit. We reasoned that in these cases, the *CI* can still be calculated because
440 it only depends on ratio of doses. We thus explored whether the role of the MEE in the initial
441 strategy developed by Chou (25) could be played by other mathematical functions. This would
442 allow fitting any shape of dose-dependent cellular responses. In addition, the absolute
443 requirement of responses ranging between 0 and 1 permitting the MEE to be applied can be
444 avoided by using other equations. The limiting ingredient to the determination of *CI* is that the
445 fitted function for the effect with respect to the dose may easily be inverted to determine Dx for
446 the observed effect fx of mixtures. It is yet important to limit the number of fitting parameters
447 in order to avoid overfitting the experimental data of the pure dose effects.

448 We thus used the set of experimental results analyzed above with the MEE equation with other
449 functions aimed at fitting the data for pure UVA and UVB and calculating Dx from fx . We first
450 applied polynomial regressions. Linear regressions were used for CPDs and 64PPs, and second
451 order polynomial regressions for Dewars. In a first attempt, second order polynomial
452 regressions were also used for 64PPs but errors were very large and the obtained *CI*s close to
453 those obtained with linear regression (data not shown). The *CI* values obtained for the four
454 CPDs, and for TT and TC 64PPs and Dewars were very similar whether a polynomic regression

455 (Table 2) or the MEE were used (Table 1). The mean ratio between values provided by the
 456 MEE and the polynomial regression is 1.06. This result shows that the *CI* can be used with any
 457 fitting function, even if it is not based on known physical-chemical processes like MEE that is
 458 based on the mass action law. In addition, the values of the level of photoproducts used in the
 459 polynomial regressions were expressed as number of photoproducts per million bases and were
 460 thus larger than 1 (up to 9000 per 10⁶ bases for TT CPD).

461 **Table 2:** Values of the combination index (*CI*) determined for increasing doses of UVA and
 462 UVB applied in an 18:1 ratio, with the use of data fitting other than the MEE. The reported
 463 total UV dose is expressed in kJ m⁻². The errors were obtained as described in the calculation
 464 section and included errors on the parameters of the polynomial regression or kinetic
 465 equations, of the *Dx* dose and on the final calculation of *CI*.

CI calculated by linear or second order polynomial regression						
UV dose	TT 64PP	TT Dewar	TC 64PP	TC Dewar	TT CPD	TC CPD
5	0.85±0.14	0.28±0.04	0.96±0.24	0.41±0.27	0.92±0.14	0.71±0.20
12	1.01±0.06	0.27±0.03	1.05±0.18	0.41±0.17	1.06±0.15	0.76±0.12
37	1.29±0.13	0.27±0.01	1.17±0.15	0.40±0.08	1.16±0.10	0.94±0.06
75	1.75±0.20	0.30±0.02	1.19±0.28	0.38±0.06	1.06±0.18	0.95±0.02
149	2.87±0.42	0.35±0.02	1.37±0.28	0.39±0.04	1.00±0.13	1.02±0.03
224	4.15±0.57	0.40±0.01	1.64±0.30	0.40±0.02	0.99±0.06	1.02±0.13
CI calculated by kinetic analysis						
UV dose	TT 64PP	TT Dewar	TC 64PP	TC Dewar	TT CPD	TC CPD
5	1.07±0.30	0.21±0.01	1.07±0.35	0.25±0.01	0.92±0.14	0.71±0.21
12	1.27±0.23	0.24±0.02	1.17±0.29	0.32±0.02	1.06±0.15	0.76±0.12
37	1.60±0.35	0.27±0.01	1.29±0.27	0.38±0.02	1.16±0.11	0.94±0.06
75	2.15±0.51	0.30±0.02	1.30±0.41	0.38±0.03	1.07±0.18	0.95±0.03
149	3.49±0.95	0.35±0.02	1.46±0.43	0.40±0.02	1.00±0.13	1.02±0.03
224	5.03±1.33	0.41±0.02	1.71±0.47	0.42±0.01	0.99±0.06	1.02±0.13

466
 467 Because the photochemical reactions leading to the formation of the three types of
 468 photoproducts are well known, we could also apply a more rigorous approach for the fit of the
 469 experimental data by using chemical kinetic equations. Formation of CPDs was described as a
 470 simple first order reaction characterized by a reaction constant *k*. In contrast, formation of 64PPs
 471 and Dewars were described as two consecutive reactions with reaction constants *k1* and *k2*. The

472 constant k_1 was related to the initial formation of 64PPs and second k_2 reflected their
473 conversion into Dewar. As described in the “Data modeling” part, these equations were used to
474 fit the data and calculate the Dx values necessary for the determination of the CI . Like for
475 polynomial regression, the obtained CI values (Table 2) were very close to those obtained using
476 the MEE (Table 1). The mean ratio between values provided by the MEE and the kinetic
477 analysis is 1.07. Obviously, this type of kinetic data analysis is only possible when the basic
478 steps of a mechanisms are well identified. In this case, the use of a strategy like the CI is thus
479 not necessary to predict occurrence of non-additivity. However, the fact that similar results
480 were obtained for the CI with various fitting strategies like MEE or polynomial regressions on
481 the one hand, and more realistic calculations based on kinetic parameters on the other, validates
482 the two former approaches. Interestingly, the kinetic analysis emphasized a limitation to the CI
483 determination that concerns all fitting functions. The dose dependent-formation of 64PPs
484 exhibits a bell-shaped curve. Calculation of the theoretical level of TT 64PP for large doses
485 based on equation (15) shows that a maximal level is reached at approximately 200 kJ m^{-2} . At
486 this dose, the level of photoproduct is 1180 TT 64PP per million bases. Consequently, above
487 this dose, the calculation of Dx will provide 2 relevant values for a mixture effect f_x and it will
488 not be possible to calculate a CI . This was not the case in our experiments where the dose was
489 lower than 12 kJ m^{-2} UVB. This example of the use of the kinetic equations illustrates that the
490 use of functions other than the MEE for the determination of CI has to be carried out at doses
491 below maximal responses for bell-shaped curves.

492 Interesting observations can also be made regarding the errors on the CI . When the latter
493 parameter was calculated on the basis of the MEE, the lowest relative errors were obtained for
494 Dewars, with values of approximately 30% at the largest dose. However, for both polynomial
495 regression and kinetic analysis, this error is on the average 5 times lower than with the MEE. A
496 similar trend was observed for 64PPs when a linear regression was used for the determination

497 of the CI compared to MEE. The relative errors on CI are 12% and 48%, respectively, for TT
498 64PP at the largest dose. The corresponding values are 19 and 50 % for TC 64PP. Comparison
499 of errors was also in favor of the kinetic analysis versus MEE, although to a lesser extent than
500 the polynomial regressions. With the kinetic analysis, the relative errors on the CI for TT 64PP
501 and TC 64PP at the largest dose were 25 and 27 %, respectively. From the back propagation
502 equations, it is possible to estimate the relative impact of the experimental data and the fitting
503 parameters on the error on Dx (ΔDx) and consequently on the CI error (ΔCI). If ΔDx is
504 dominated by the parameters of the fits, other fitting functions may require to be considered or
505 experiments of pure factors with a larger dose range. On the contrary, if ΔDx is dominated by
506 experimental data on mixture effects, new experiments of mixtures with more replicates may
507 be required. For TT 64PP at the largest dose, ΔDx determined with the MEE originates in 42%,
508 32% and 26% from error on Dm , m and fx , respectively. In this case, improvement of the
509 accuracy of the fit seems necessary. For the kinetic analysis approach applied to TT 64PP, the
510 proportions of ΔDx originating from $k1$, $k2$ and fx were 22%, 31% and 47% at the largest dose.
511 The result show a strong contribution of the fit. For the second order polynomial fit of TT 64PP
512 (not discussed in this work), ΔCI was 2000 for a CI of 4.5 and the error on the quadratic
513 coefficient represented 99.9% of ΔDx . With the linear regression, a much lower error was
514 obtained (0.57). The contribution of the errors to ΔDx were 14 and 86 % for the value of the
515 slope and fx , respectively. In this case, increasing the quality of the experimental results of
516 mixtures, for example by using more replicates, could improve the estimation of CI . The second
517 order polynomial fit was found to be very accurate for TT Dewar with an error of 4% on CI at
518 the largest dose. In this case the contribution of the errors to ΔDx were 40%, 56% and 4% for
519 quadratic term, the linear term and fx , respectively. These observations point again to a
520 significant contribution of the quality of the fit to the error on the CI . Altogether, these results
521 suggests that ΔDx and ΔCI are mostly explained by errors on the fit, especially when the overall

522 errors are large. This shows that the choice of the fitting function is a key parameter in the
523 accuracy of the determination of the *CI*. In the average, the MEE predicts *CI* with an error on
524 the average 4 times larger than polynomial regressions or kinetic analysis, while the *CI* values
525 are similar with all approaches.

526

527 **Dependence of *CI* on the irradiation conditions**

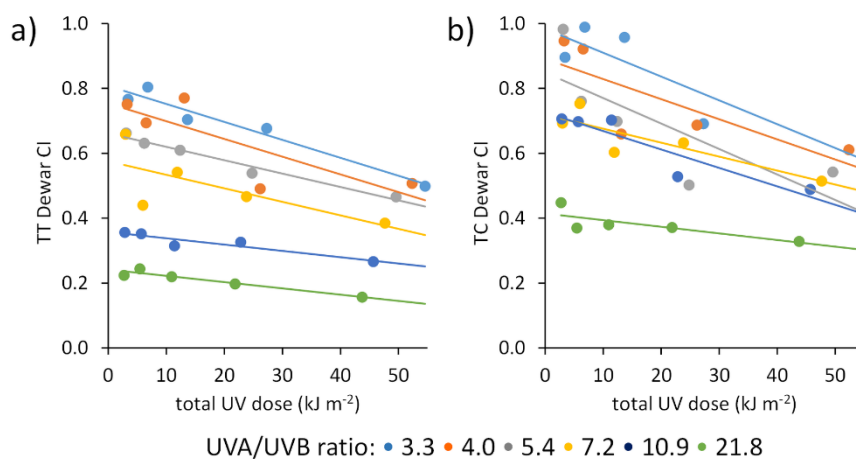
528 We then performed a series of experiments still involving a combination of UVA and UVB in
529 order to determine whether the *CI* was sensitive to the exposure protocols. In this experiment
530 and in all the rest of the work, we relied on the initial strategy designed by Chou et al. (25, 27)
531 for the calculation of the *CI* with the MEE. We first investigated whether the *CI* varied
532 according to the UVA/UVB ratio. We then studied the impact of the order in which UVA was
533 combined with UVB, either simultaneously or one after the other. For these experiments, only
534 one sample was collected at each dose. Consequently, we did not calculate errors.

535 *Evolution of the *CI* at different UVA to UVB ratios*

536 In the previous study, UVA and UVB were applied at a constant ratio of 18:1. Yet, it is
537 anticipated that the efficiency of conversion of 64PPs into Dewars depends on the relative
538 intensities of UVB and UVA. Therefore, we calculated the *CI* through a MEE fitting for
539 different exposure conditions exhibiting increasing UVA to UVB ratios. For this purpose, we
540 kept the UVA fluence constant and decreased that of the UVB source. The results
541 unambiguously showed a decrease of the value of the *CI* related to Dewars with increasing
542 ratio, namely an increase in the synergistic effect, when the UVA to UVB ratio increased (Fig.
543 3). Conversely, the *CI* for TT and TC 64PPs was larger than 1 under all exposure conditions,
544 showing the antagonist effect of UVA. The effect was not as strong as those shown on Figure
545 1 because the total UV doses applied were lower. Like in our experiments at constant

546 UVA/UVB ratio, the values of the *CI* for TC Dewar were larger than those for the TT Dewar.
 547 The mean ratio between the *CI* of TC Dewar and TT Dewar at different applied doses ranged
 548 from 1.2 for a UVA/UVB ratio of 3.3, to 1.9 for a UVA/UVB ratio of 21.8. These observations
 549 reflect the more efficient isomerization of TT 64PP in the UVA range compared to TC 64PP.
 550 This experiment illustrates that the *CI* is more than a semi-quantitative indication of the
 551 non-additivity of response in co-exposures. The modulation of DNA photochemistry induced
 552 by changing the ratio between the fluence of UVB and UVA by a value of 2 or 3 was enough
 553 to be reflected in the values of the *CI*.

554



555
 556 **Figure 3:** Value of the *CI* for a) TT Dewar and b) TC Dewar in DNA samples exposed to
 557 radiation with various UVA/UVB ratios.

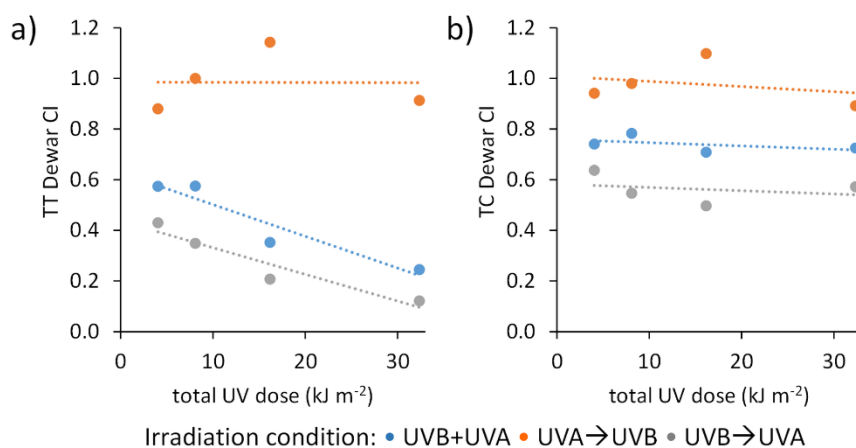
558

559

560 ***Effect of the order of exposure on the value of CI***

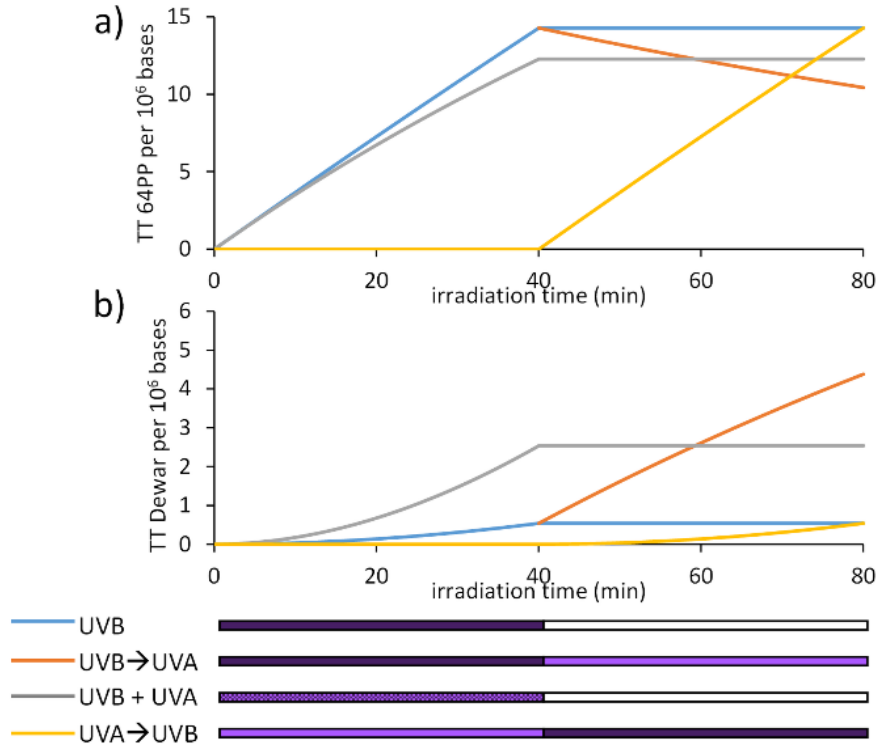
561 In the subsequent study, we compared the results of UVB and UVA co-exposure experiments
 562 where the two radiation ranges were applied either simultaneously or one after the other.
 563 Experiments involving pure UVA and UVB were also performed in order to calculate the *CI*.
 564 As observed in all the other experiments, the *CI* values determined for CPDs were close to 1,

565 irrespectively of the irradiation conditions and of the dose (data not shown). Interestingly, the
566 total dose of UVA and UVB received by the DNA samples was the same in the UVA→UVB,
567 UVB+UVA and UVB→UVA protocols. Yet, differences were observed in the
568 photoisomerization yield. In the first case (UVA→UVB), the efficiency is not different than
569 with UVB alone as shown by the *CI* close to 1 for 64PPs and Dewars. This is expected since
570 UVA is applied first and cannot be absorbed by 64PPs produced by UVB. This was not the case
571 for the two other irradiation protocols. For TT 64PP, the value of the *CI* increased continuously
572 from 0.98 to 1.30 with increasing dose for UVB+UVA and from 1.26 to 1.69 for UVB→UVA.
573 The same trend was observed for TC 64PP. The *CI* values obtained at the lowest and largest
574 UV doses were 1.00 to 1.14 with increasing dose for UVB+UVA and from 1.04 to 1.29 for
575 UVB→UVA. A mirror effect was observed on the Dewar data. As shown on figure 4, the *CI*
576 value for both TT and TC Dewars were 1 on the average in the UVA→UVB protocol, but lower
577 in the UVB+UVA and UVB→UVA experiments. The mean values are 0.44 and 0.28 for TT
578 Dewar for UVB+UVA and UVB→UVA, respectively. The corresponding values for TC Dewar
579 are 0.74 and 0.56. (Fig. 4). In summary, the *CI* for 64PPs was larger for UVB→UVA than
580 UVB+UVA while the opposite trend was observed for Dewars. Interestingly, the *CI* of the TT
581 64PP is more dose-dependent than that of TC 64PP. This can be explained by the fact that the
582 photoisomerization reaction is more efficient. Consequently, the trend to a plateau for 64PP and
583 the quadratic shape of the formation of Dewar are more pronounced for TT than TC. In the
584 calculation of the *CI*, this is reflected by a larger dose dependence for TT than TC
585 photoproducts.



586
 587 **Figure 4:** variation of CI of TT and TC Dewars for different irradiation protocols. UVB and
 588 UVA were applied simultaneously (UVB+UVA), or successively UVB → UVA or UVA →UVB.
 589 Dashed lines are linear fits to illustrate the trends of CI as function of the total UV dose.

590
 591 The bulk of these observations unambiguously shows that the photoisomerization is more
 592 efficient with UVB→UVA than UVB+UVA. This result can be explained by the fact that when
 593 UVA is applied after UVB, all UVB-induced 64PPs absorb the maximal amount of UVA. When
 594 both wavelength ranges are applied simultaneously, the same amount of 64PPs as in the
 595 UVB→UVA design are produced. However, those formed close to the end of irradiation are
 596 exposed to a lower dose of UVA than those produced at the beginning. Consequently, their
 597 yield of photoisomerization is lower. A more comprehensive explanation can be found in figure
 598 5 that shows, for the 40 min experiments, the evolution of the level of TT 64PP and TT Dewar
 599 under the different exposure protocols. The x-scale of the graph is in min because total UV
 600 doses are quite different for UVB alone and combination of UVB and UVA. CI reported in
 601 figure 4 were the final values for each irradiation time (5+5, 10+10, 20+20 or 40+40 min).



602

603 **Figure 5:** Formation of a) TT 64PP and b) TT Dewar in isolated DNA exposed to either UVB

604 alone or to UVB and UVA in different combinations. UVB+UVA: simultaneous exposure;

605 UVB → UVA: UVB alone followed by UVA alone; UVA → UVB: UVA alone followed by UVB

606 alone. The graphs were obtained by using equations (14) and (15). The value of k_1 was

607 obtained in the UVB experiment. A value k_{2UVB} was determined for pure UVB as explained in

608 the calculation part. A similar approach was applied for the determination of $k_{2UVB+UVA}$ in the

609 UVB+UVA experiment. The difference between these 2 values yielded k_{UVA} used for the fit of

610 the UVB → UVA data. The values of k_1 , k_{2UVB} , $k_{2UVB+UVA}$ and k_{2UVA} were found to be $4 \cdot 10^{-7}$,

611 0.002 , 0.010 and 0.008 min^{-1} , respectively.

612

613

614 Combination of 3 UV sources

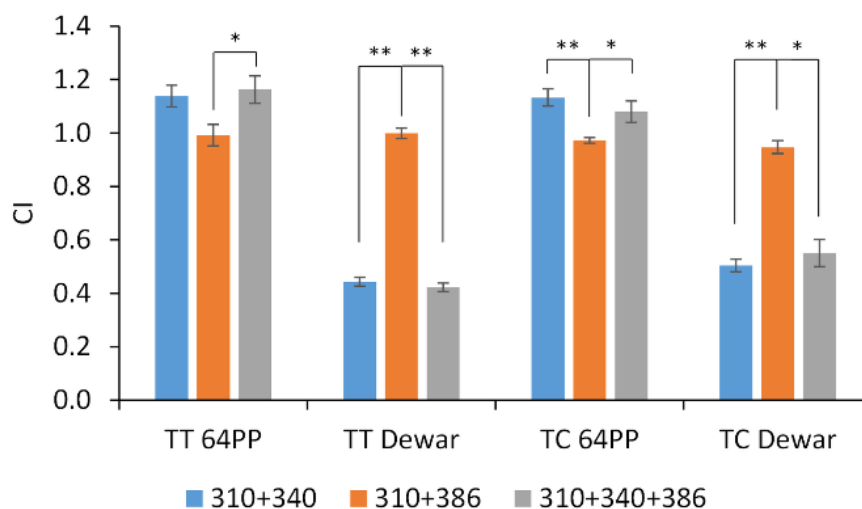
615 The results presented above involved only a UVB and a UVA source. Yet, photobiological

616 processes could be modulated by combinations of more than 2 ranges of wavelengths. We took

617 advantage that the CI can be used with more than two factors to explore a ternary combination

618 of UV radiation. Using our exposure device fitted with specific filters, we exposed DNA to

619 UVB (310±5 nm), UVA2 (340±13 nm) and UVA1 (386±13.5 nm). In addition to each radiation
620 alone and to the ternary combination, we exposed solutions of isolated DNA to a combination
621 of UVB and UVA2 (310+340 nm) and a combination of UVB and UVA1 (310+386 nm). As
622 observed with the full UVA spectrum, neither UVA1 nor UVA2 led to the formation of 64PPs
623 and Dewars. We observed that the *CI* was 1 for 64PPs and Dewars for the 310+386 nm
624 combination (Fig. 6), suggesting that UVA1 is not efficient in the photoisomerization of 64PP.
625 In contrast, the *CI* for Dewars in the 310+340 nm experiments were below 0.5 and statistically
626 significantly lower than those observed for 310+386 nm. The same observations were made in
627 the ternary combination, showing that addition of UVA1 to the UVB/UVA2 radiation did not
628 increase the photoisomerization yield of 64PPs. It should be noticed that a statistically
629 significant larger *CI* was obtained for TC 64PP in the 310+340 nm irradiation compared to
630 310+386, as well as between the 310+386 and the 310+340+386 experiments. The latter
631 difference was also statistically significant for TT 64PP, and the comparison between 310+340
632 and 310+386 exhibited the same trend of a *CI* closer to 1 under the latter condition. These
633 results strongly suggest an antagonist effect of UVA2, but not of UVA1, on the formation of
634 64PPs. Combined with observation of synergistic effects of UVA2 but not UVA1 on the
635 formation of Dewars, the *CI* analysis allowed us to conclude that UVA1 does not participate to
636 the photoisomerization of 64PPs, in agreement with their known absorption properties.



637
 638 **Figure 6:** *CI determined for TT and TC 64PPs and Dewars in DNA samples exposed to*
 639 *combination of UVB, UVB and UVA1 and UVB and UVA2. The reported results are means ±*
 640 *SEM determined in triplicate at 4 different total UV doses (n=12). The statistical significance*
 641 *of the differences, evaluated by a one-way ANOVA, were $p < 0.05$ (*) or $p < 0.01$ (**).*

642

643 CONCLUSION

644 In the present work, we proposed the use of the combination index as a tool to identify non
 645 additive effects upon co-exposure to different radiation ranges. Application of this approach to
 646 the well-known photochemistry of DNA shows that the *CI* strategy is as efficient with light as
 647 it is with chemicals. We also provided some improvements to the original design by showing
 648 that fitting functions other than the MEE can be used. In particular, we show that regressions
 649 that are not necessarily based on physico-chemical principles like the mass action law for MEE
 650 or chemical kinetics analysis are well suited. In our case, linear and second order polynomial
 651 fits of the data provided *CI* values similar to those obtained with the MEE or kinetic analysis,
 652 with the lowest incertitude. In addition, these fitting functions can exhibit any dose-response
 653 curves, except bell-shaped responses. Another advantage of the use of such fitting functions is
 654 that the value of the considered effect does not have to be lower than 1 as in the MEE, which

655 would be a strong limitation for example for the induction of all photobiological effects
656 normalized to a control like gene expression or protein synthesis. Further developments will
657 involve application of the combination index strategy to investigations of the effect of complex
658 exposures on living systems with biologically relevant endpoints. Another long term project
659 would be to incorporate the non-additivity brought by *CI* methodology in a generalized action
660 spectra for the estimation of dose effects with complex light sources like solar spectra.

661

662 **ACKNOWLEDGMENTS**

663 This work was supported by the Labex ARCANE and the CBH-EUR-GS
664 (ANR-17-EURE-0003).

665 **REFERENCES**

666

- 667 1. Björn, L. O. (2015) Action spectroscopy in biology. In *Photobiology: The Science of Light*
668 *and Life*. (Edited by L. O. Björn), pp. 85-96. Springer Science + Business Media, New-
669 *York*.
- 670 2. Sliney, D. H. (2006) Photobiological measurements and obtaining action spectra. In *Cell*
671 *Biology and Instrumentation: UV Radiation, Nitric Oxide, and Cell Death in Plants*
672 (Edited by Y. Blume, D. J. Durzan and P. Smertenko), pp. 11-26. IOS Press,
673 *Amsterdam*.
- 674 3. Setlow, R. (1957) Action spectroscopy. *Adv. Biol. Medic. Phys.* **5**, 37-74.
- 675 4. Schäfer, E. and L. Fukshansky (1984) Action spectroscopy. In *Techniques in*
676 *Photomorphogenesis*. (Edited by H. Smith and M. G. Holmes). Academic Press, New-
677 *York*.
- 678 5. Withrow, R. B., W. H. Klein and V. Elstad (1957) Action Spectra of Photomorphogenic
679 *Induction and Its Photoinactivation. Plant Physiol.* **32**, 453-462.
- 680 6. Essen, L. O. and T. Klar (2006) Light-driven DNA repair by photolyases. *Cell. Mol. Life Sci.*
681 **63**, 1266-1277.
- 682 7. Weber, S. (2005) Light-driven enzymatic catalysis of DNA repair: a review of recent
683 *biophysical studies on photolyase. Biochim. Biophys. Acta* **1707**, 1-23.

- 684 8. Douki, T. (2021) Wavelengths and temporal effects on the response of mammalian cells to
685 UV radiation: Limitations of action spectra illustrated by genotoxicity. *J Photochem*
686 *Photobiol B* **217**, 112169.
- 687 9. Damian, D. L., Y. J. Matthews, T. A. Phan and G. M. Halliday (2011) An action spectrum
688 for ultraviolet radiation-induced immunosuppression in humans. *Br. J. Dermatol.* **164**,
689 657-659.
- 690 10. Garssen, J., F. de Gruijl, D. Mol, A. de Klerk, P. Roholl and H. Van Loveren (2001) UVA
691 exposure affects UVB and cis-urocanic acid-induced systemic suppression of immune
692 responses in *Listeria monocytogenes*-infected balb/c mice. *Photochem. Photobiol.* **73**,
693 432-438.
- 694 11. Reeve, V. E., M. Bosnic, C. Boehm-Wilcox, N. Nishimura and R. D. Ley (1998) Ultraviolet
695 A radiation (320-400 nm) protects hairless mice from immunosuppression induced by
696 ultraviolet B radiation (280-320 nm) or cis-urocanic acid. *Int. Arch. Allergy Immunol.*
697 **115**, 316-322.
- 698 12. Tuchinda, C., H. W. Lim, F. M. Strickland, E. A. Guzman and H. K. Wong (2007)
699 Comparison of broadband UVB, narrowband UVB, broadband UVA and UVA1 on
700 activation of apoptotic pathways in human peripheral blood mononuclear cells.
701 *Photodermatol. Photoimmunol. Photomed.* **23**, 2-9.
- 702 13. Ibuki, Y., Y. Komaki, G. Yang and T. Toyooka (2021) Long-wavelength UVA enhances
703 UVB-induced cell death in cultured keratinocytes: DSB formation and suppressed
704 survival pathway. *Photochem Photobiol Sci* **20**, 639-652.
- 705 14. Tonolli, P. N., O. Chiarelli-Neto, C. Santacruz-Perez, H. C. Junqueira, I. S. Watanabe, F.
706 G. Ravagnani, W. K. Martins and M. S. Baptista (2017) Lipofuscin generated by UVA
707 turns keratinocytes photosensitive to visible light. *J. Invest. Dermatol.* **137**, 2447-2450.
- 708 15. Dreaden, T. M., J. Chen, S. Rexroth and B. A. Barry (2011) N-formylkynurenine as a
709 marker of high light stress in photosynthesis. *J. Biol. Chem.* **286**, 22632-22641.
- 710 16. Park, S. L., R. Justiniano, J. D. Williams, C. M. Cabello, S. Qiao and G. T. Wondrak (2015)
711 The tryptophan-derived endogenous aryl hydrocarbon receptor ligand 6-
712 formylindolo[3,2-b]carbazole is a nanomolar UVA photosensitizer in epidermal
713 keratinocytes. *J. Invest. Dermatol.* **135**, 1649-1658.
- 714 17. Walrant, P. and R. Santus (1974) N-formyl-kynurenine, a tryptophan photooxidation
715 product, as a photodynamic sensitizer. *Photochem. Photobiol.* **19**, 411-417.
- 716 18. Douki, T. and E. Sage (2015) Dewar valence isomers, the third type of environmentally
717 relevant DNA photoproducts induced by solar radiation. *Photochem. Photobiol. Sci.* **15**,
718 24-30.
- 719 19. Taylor, J.-S. and M. P. Cohrs (1987) DNA, light, and Dewar pyrimidones: the structure and
720 biological significance of TpT3. *J. Am. Chem. Soc.* **109**, 2834-2835.
- 721 20. Escher, B. I., J. Hackermuller, T. Polte, S. Scholz, A. Aigner, R. Altenburger, A. Bohme,
722 S. K. Bopp, W. Brack, W. Busch, M. Chadeau-Hyam, A. Covaci, A. Eisentrager, J. J.
723 Galligan, N. Garcia-Reyero, T. Hartung, M. Hein, G. Herberth, A. Jahnke, J. Kleinjans,
724 N. Kluver, M. Krauss, M. Lamoree, I. Lehmann, T. Luckenbach, G. W. Miller, A.
725 Muller, D. H. Phillips, T. Reemtsma, U. Rolle-Kampczyk, G. Schuurmann, B.
726 Schwikowski, Y. M. Tan, S. Trump, S. Walter-Rohde and J. F. Wambaugh (2017) From
727 the exposome to mechanistic understanding of chemical-induced adverse effects.
728 *Environ. Int.* **99**, 97-106.

- 729 21. Lasch, A., D. Lichtenstein, P. Marx-Stoelting, A. Braeuning and J. Alarcán (2020) Mixture
730 effects of chemicals: The difficulty to choose appropriate mathematical models for
731 appropriate conclusions. *Environ. Pollut.* **260**, 113953.
- 732 22. Olmstead, A. W. and G. A. LeBlanc (2005) Toxicity assessment of environmentally
733 relevant pollutant mixtures using a heuristic model. *Integr. Environ. Assess. Manag.* **1**,
734 114-122.
- 735 23. Rider, C. V. and G. A. LeBlanc (2005) An integrated addition and interaction model for
736 assessing toxicity of chemical mixtures. *Toxicol Sci* **87**, 520-528.
- 737 24. Chou, T. C. and P. Talalay (1984) Quantitative-Analysis of Dose-Effect Relationships - the
738 Combined Effects of Multiple-Drugs or Enzyme-Inhibitors. *Adv. Enzyme Regul.* **22**, 27-
739 55.
- 740 25. Chou, T. C. (2006) Theoretical basis, experimental design, and computerized simulation of
741 synergism and antagonism in drug combination studies. *Pharmacological Reviews* **58**,
742 621-681.
- 743 26. Chou, T. C. (2008) Preclinical versus clinical drug combination studies. *Leuk. Lymphoma*
744 **49**, 2059-2080.
- 745 27. Chou, T. C. (2011) The mass-action law based algorithm for cost-effective approach for
746 cancer drug discovery and development. *Am. J. Cancer Res.* **1**, 925-954.
- 747 28. Cadet, J. and T. Douki (2018) Formation of UV-induced DNA damage contributing to skin
748 cancer development. *Photochem. Photobiol. Sci.* **17**, 1816-1841.
- 749 29. Douki, T. (2006) Effect of denaturation on the photochemistry of pyrimidine bases in
750 isolated DNA. *J. Photochem. Photobiol. B: Biol.* **82**, 45-52.
- 751 30. Douki, T. (2016) Sunlight-induced DNA damage: molecular mechanisms and
752 photoprotection strategies. In *Skin Stress Response Pathways: Environmental Factors*
753 *and Molecular Opportunities*. (Edited by G. T. Wondrak), pp. 49-77. Springer Int.
754 Publish.
- 755 31. Douki, T., L. Voituriez and J. Cadet (1991) Characterization of the (6-4) photoproduct of
756 2'-deoxycytidylyl-(3'-5')-thymidine and of its Dewar valence isomer. *Photochem.*
757 *Photobiol.* **27**, 293-297.
- 758 32. Taylor, J.-S., H.-L. Lu and J. J. Kotyk (1990) Quantitative conversion of the (6-4)
759 photoproduct of TpdC to its Dewar valence isomer upon exposure to simulated sunlight.
760 *Photochem. Photobiol.* **51**, 161-167.
- 761 33. Lemaire, D. G. E. and B. P. Ruzsicska (1993) Quantum yields and secondary photoreactions
762 of the photoproducts of dTpdT, dTpdC and dTpdU. *Photochem. Photobiol.* **57**, 755-
763 769.
- 764 34. Douki, T. (2016) Relative contributions of UVB and UVA to the photoconversion of (6-4)
765 photoproducts into their Dewar valence isomers. *Photochem. Photobiol.* **92**, 587-594.
- 766 35. Douki, T. (2013) The variety of UV-induced pyrimidine dimeric photoproducts in DNA as
767 shown by chromatographic quantification methods. *Photochem. Photobiol. Sci.* **12**,
768 1286-1302.
- 769 36. Matallana-Surget, S., J. A. Meador, F. Joux and T. Douki (2008) Effect of the GC content
770 of DNA on the distribution of UVB-induced bipyrimidine photoproducts. *Photochem.*
771 *Photobiol. Sci.* **7**, 794-801.
- 772 37. Douki, T., I. Berard, A. Wack and S. Andra (2014) Contribution of cytosine-containing
773 cyclobutane dimers to DNA damage produced by photosensitized triplet-triplet energy
774 transfer. *Chem. Eur. J.* **20**, 5787-5794.

- 775 38. Tuckerman, M. E. (2019) Chemical Kinetics - More complex reactions. In *Physical*
776 *chemistry for the biosciences*. pp. 9.4.1-9.4.6. LibreTexts.
- 777 39. Courdavault, S., C. Baudouin, M. Charveron, A. Favier, J. Cadet and T. Douki (2004)
778 Larger yield of cyclobutane dimers than 8 oxo-7,8-dihydroguanine in the DNA of UVA-
779 irradiated human skin cells. *Mutat. Res.* **556**, 135-142.
- 780 40. Mouret, S., C. Baudouin, M. Charveron, A. Favier, J. Cadet and T. Douki (2006)
781 Cyclobutane pyrimidine dimers are predominant DNA lesions in whole human skin
782 exposed to UVA radiation. *Proc. Natl. Acad. Sci. USA* **103**, 13765-13770.
- 783 41. Mouret, S., C. Philippe, J. Gracia-Chantegrel, A. Banyasz, S. Karpati, D. Markovitsi and T.
784 Douki (2010) UVA-induced cyclobutane pyrimidine dimers in DNA: a direct
785 photochemical mechanism? *Org. Biomolec. Chem.* **8**, 1706-1711.
- 786 42. Johns, H. E., S. A. Rapaport and M. Delbück (1962) Photochemistry of thymine dimers. *J.*
787 *Mol. Biol.* **4**, 104-114.
- 788 43. Lemaire, D. G. E. and B. P. Ruzsicska (1993) Kinetic analysis of the deamination reactions
789 of cyclobutane dimers of thymidylyl-3',5'-2'-deoxycytidine and 2'-deoxycytidine-3,5'-
790 thymidine. *Biochemistry* **32**, 2525-2533.
- 791 44. Douki, T. and J. Cadet (2001) Individual determination of the yield of the main-UV induced
792 dimeric pyrimidine photoproducts in DNA suggests a high mutagenicity of CC
793 photolesions. *Biochemistry* **40**, 2495-2501.
- 794 45. Clingen, P. H., C. F. Arlett, L. Roza, T. Mori, O. Nikaido and M. H. L. Green (1995)
795 Induction of cyclobutane pyrimidine dimers, pyrimidine(6-4)pyrimidone
796 photoproducts, and Dewar valence isomers by natural sunlight in normal human
797 mononuclear cells. *Cancer Res.* **55**, 2245-2248.
- 798 46. Qin, X. S., S. M. Zhang, M. Zarkovic, Y. Nakatsuru, S. Shimizu, Y. Yamazaki, H. Oda, O.
799 Nikaido and T. Ishikawa (1996) Detection of ultraviolet photoproducts in mouse skin
800 exposed to natural sunlight. *Jap. J. Cancer Res.* **87**, 685-690.
- 801 47. Meador, J. A., A. J. Baldwin, J. D. Pakulski, W. H. Jeffrey, D. L. Mitchell and T. Douki
802 (2014) The significance of the Dewar valence photoisomer as a UV radiation-induced
803 DNA photoproduct in marine microbial communities. *Environm. Microbiol.* **16**, 1808-
804 1820.
- 805 48. Douki, T., T. Zalizniak and J. Cadet (1997) Far-UV-induced dimeric photoproducts in short
806 oligonucleotides: Sequence effects. *Photochem. Photobiol.* **66**, 171-179.
- 807